Physics of the Earth and Planetary Interiors 301 (2020) 106450

Contents lists available at ScienceDirect

Physics of the Earth and Planetary Interiors

journal homepage: www.elsevier.com/locate/pepi

A squirt-flow theory to model wave anelasticity in rocks containing compliant microfractures

Chunfang Wu[a,b], Jing Ba[a,*], José M. Carcione[a,c], Li-Yun Fu[d], Evgeni M. Chesnokov[b], Lin Zhang[a]

[a] School of Earth Sciences and Engineering, Hohai University, Nanjing, PR China
[b] Department of Earth and Atmospheric Sciences, University of Houston, Houston, TX 77204, USA
[c] Istituto Nazionale di Oceanografia e di Geofisica Sperimentale (OGS), Trieste 34010, Italy
[d] School of Geosciences, China University of Petroleum (East China), Qingdao 266580, China

ARTICLE INFO

Keywords:
Squirt-flow model
Microfracture
Velocity dispersion
Attenuation
Wave propagation
Poroelasticity

ABSTRACT

Wave propagation in rocks induces fluid pressure gradients and flow between stiff intergranular pores and compliant microfractures. This, in turn, leads to wave anelasticity, i.e., attenuation and velocity dispersion. Three known squirt-flow models attempt to explain this phenomenon. Based on these theories, we reformulate a new one, where we derive the dry-rock moduli on the assumption that the boundary fluid pressure is constant. The new model improves the predictions of the other models, e.g., a better description at high frequencies and the inclusion of permeability effects. The numerical example shows the response due to the characteristic squirt-flow length and fluid viscosity on wave propagation. The reformulated model is applied to experiments made on water-saturated tight sandstones, where the squirt-flow length is determined, showing that it increases with increasing permeability and porosity at full saturation.

1. Introduction

Microfractures and grain contacts (cracks) are generated in diagenesis processes of sedimentary rocks during geological time. These microcracks/microfractures are flat and soft, i.e., having a low aspect ratio, and with much higher compressibilities than the primary intergranular stiff pores. A P wave induces fluid pressure gradients and squirt flow between cracks and stiff pores, due to their different compressibilities. This local flow induces, in turn, velocity dispersion and attenuation (Carcione, 2014; Müller et al., 2010). To model this phenomenon, Biot (1962) proposed a viscoelastic mechanical model to describe it. Quoting Biot: "When two elastic bodies are in contact and are surrounded by a viscous fluid, a force applied in a direction normal to the area of contact will tend to squeeze the flow away from this area. Because of fluid viscosity, the fluid will not move away instantaneously. A time delay, which is exemplified by the equivalent spring dashpot model, will be involved." This model is the Zener or standard-linear solid mechanical model (e.g., Carcione, 2014).

Wave velocity dispersion due to squirt flow was observed in ultrasonic experiments on sandstones (Winkler, 1983; Han, 1986; Han et al., 1986; Wang and Nur, 1990). Winkler (1983) has not detected significant dispersion in artificial sintered glass beads. Mavko and Jizba (1994) evaluated the bulk and shear moduli dispersion in forty rock samples (Coyner, 1984; Han, 1986; Han et al., 1986). Comparing the predictions with the Gassmann (1951), Biot (1956a, 1956b, 1962) and Mavko and Jizba (1991) models, they concluded that most of the observed dispersion can be explained by the squirt-flow mechanism.

The squirt-flow model was further studied by Dvorkin and Nur (1993) and Dvorkin et al. (1994), in the framework of the Biot theory (the so-called BISQ model). The BISQ model predicts more dispersion than the classical Biot theory, with a lower velocity at low frequencies, compared to Gassmann equation, and it is consistent with Biot prediction at high frequencies. Dvorkin et al. (1995) modified the theory to be consistent with Gassmann moduli at low frequencies, assuming effective dry-rock moduli, where the cracks are part of the skeleton. Then, Gurevich et al. (2009, 2010) obtained an alternative expression of the dry-rock moduli based on the theory of Murphy et al. (1986), which can be applied to gas-saturated rocks at all frequencies. Using this model, Markova et al. (2014) investigated the effect of squirt flow and macroscopic seepage on acoustic logging signals. Carcione and Gurevich (2011) unified the squirt-flow and Biot theories and showed that the new model can be represented with Zener kernels under certain conditions of the fluid properties, as Biot (1962) has predicted. Yang and Zhang (2000, 2002) proposed an extension to the anisotropy case.

Alternative theories are based on the concept of double porosity (Pride and Berryman, 2003; Pride et al., 2004; Ba et al., 2011, 2014,

* Corresponding author.
E-mail address: jingba@188.com (J. Ba).

https://doi.org/10.1016/j.pepi.2020.106450
Received 14 January 2020; Received in revised form 19 February 2020; Accepted 19 February 2020
Available online 20 February 2020
0031-9201/

2017, 2019; Zhang et al., 2019), where the fluid flow is also due to pressure gradients between regions of soft and stiff pores, and the wave propagation governing equations are derived by incorporating two pore phases and one solid skeleton. Other models can be found in Tang et al. (2012) and Yao et al. (2015).

In the present paper, we reformulate the squirt-flow theory, based on Dvorkin et al. (1995), by applying the boundary condition of Gurevich et al. (2010). P-wave velocity obtained from the new theory is consistent with that from the Gassmann model at the low frequency limit, and it approaches to the high limit value (the rock without compliant pores) at high frequencies, when the model parameters are the same as those of Dvorkin et al. (1995). The change of permeability affects the squirt flow characteristic frequency. We compare the different models and then apply the new one to explain pressure-dependent experimental data of ultrasonic measurements in tight-sandstones.

2. Squirt-flow models

The models proposed by Dvorkin et al. (1995), Gurevich et al. (2010) and Carcione and Gurevich (2011) are outlined in this section. Let us refer to them as models 1, 2 and 3, respectively. The medium is isotropic and the pore space is divided into compliant pores (microfractures, grain contacts, cracks) and stiff pores (intergranular voids).

2.1. Model 1

A modified frame is generated (see Fig. 1), which contains only stiff pores. Following Mavko and Jizba (1991), Dvorkin et al. (1995) derived the wet-rock bulk (K_r) and shear moduli (μ_r) of the modified frame as

$$K_r = \frac{K_m}{1 + \alpha_m \mathrm{d}P/\mathrm{d}\sigma}, \tag{1a}$$

$$\frac{1}{\mu_r} = \frac{1}{\mu_{dry}} - \frac{4}{15}\left(\frac{1}{K_{dry}} - \frac{1}{K_{md}}\right), \tag{1b}$$

where K_{dry} and μ_{dry} are the dry-rock bulk and shear moduli, respectively, K_m is the bulk modulus of the modified frame, α_m is the modified poroelasticity coefficient, K_{md} is the bulk modulus of the modified dry frame, when the microfractures are saturated and the stiff pores are empty, $_P$ is the pore pressure and σ is the total pressure. The P-wave velocity predicted by this model is consistent with Gassmann moduli at the low frequencies (Dvorkin et al., 1995).

2.2. Model 2

Gurevich et al. (2010) employed the geometric model presented by Murphy et al. (1986): A compliant pore forms a disk-shaped gap between the two adjacent grains, and its edge opens into a toroidal stiff pore. In addition, the fluid motion does not affect its geometry (Fig. 2). By considering that the pressure is zero at the edge of the gap ($r = a$), the additional effective stiffness is calculated based on the fluid mass conservation, which is

$$K^*(p, w) = \left[1 - \frac{2J_1(ka)}{ka J_0(ka)}\right] K_{fl}, \tag{2}$$

where $ka = 1/\gamma(-3i\omega\eta/K_{fl})^{1/2}$,$\omega$ is the angular frequency, η is the fluid viscosity, a is the gap radius, h is the gap thickness, $\gamma = h/(2a)$ is the aspect ratio of the soft pores, K_{fl} is the fluid bulk modulus, and J_0 and J_1 are the zero- and first-order Bessel functions, respectively.

Then, the bulk (K_{md}) and shear moduli (μ_{md}) of the modified dry frame are:

$$\frac{1}{K_{md}} = \frac{1}{K_{hp}} + \frac{1}{\frac{1}{\frac{1}{K_{dry}} - \frac{1}{K_{hp}}} + \frac{1}{\left(\frac{1}{K^*} - \frac{1}{K_0}\right)\phi_c}}, \tag{3a}$$

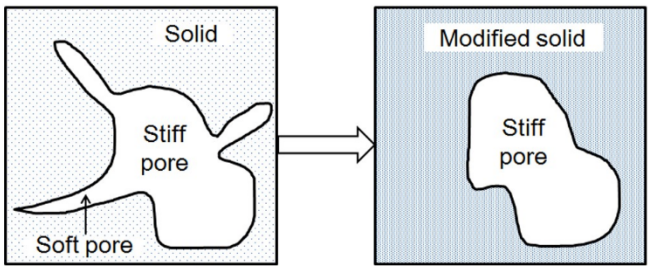

Fig. 1. Modified rock skeleton.

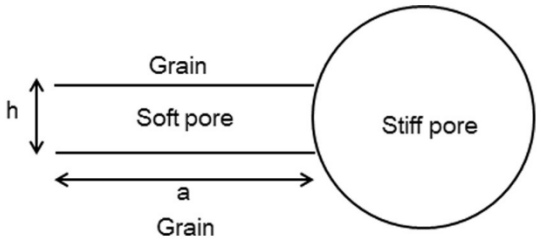

Fig. 2. Idealized geometry of soft and stiff pores (Murphy et al., 1986).

$$\frac{1}{\mu_{md}} = \frac{1}{\mu_{dry}} - \frac{4}{15}\left[\frac{1}{K_{dry}} - \frac{1}{K_{md}}\right], \tag{3b}$$

where K_{hp} is the dry-rock bulk modulus when all the microfractures are closed, i.e., the high-pressure modulus (e.g., Berryman, 2007), K_0 is the bulk modulus of the mineral, and ϕ_c is the compliant-pore porosity. The P-wave velocity predicted by this model is consistent with Gassmann equation at the low frequency limit. However, the model neglects the effect of permeability. In the other models, the characteristic frequency of the squirt-flow dissipation peak moves to high frequencies as permeability increases (Dvorkin and Nur, 1993; Parra, 1997).

2.3. Model 3

Based on Gurevich et al. (2009, 2010), Carcione and Gurevich (2011) showed that squirt-flow differential equations of motion are those of the Biot theory of poroelasticity combined with a set of Zener viscoelastic models. They solved the equations for heterogeneous media by using a time-splitting technique and the Fourier pseudo-spectral method, to compute synthetic seismograms.

The Zener modulus is

$$Z = Z(M_R, \tau_\varepsilon, \tau_\sigma) = M_R\left(\frac{1 + i\omega\tau_\varepsilon}{1 + i\omega\tau_\sigma}\right), \tag{4}$$

where M_R is the relaxation modulus, τ_ε is the strain relaxation time and τ_σ is the stress relaxation time. Eq. (4) is a mechanical model that consists of two springs and one dashpot (Carcione, 2014). The modified dry-rock moduli by Gurevich et al. (2010) can exactly be represented by the Zener mechanical model. The P-wave phase velocity and dissipation factor are:

$$V_{phP} = \left[\mathrm{Re}\left(\frac{1}{V_P^2}\right)\right]^{-1}, \tag{5}$$

$$Q^{-1} = \frac{\mathrm{Im}(V_P^2)}{\mathrm{Re}(V_P^2)} \tag{6}$$

respectively. The complex P-wave velocity (V_P) can then be obtained from the following equation:

$$\rho_2\rho_1 V_P^4 + a_1 V_P^2 + a_0 = 0 \tag{7}$$

where $a_1 = (2\alpha_0\rho_{fl} - \rho)M - \rho_1\left(K_G + \frac{4}{3}\mu_G\right)$, $a_0 = (K + 4\mu_G/3)M$, and M, K_G, K, and μ_G are obtained from the Zener model. $\alpha_0 = 1 - K_{dry}/K_0$, ρ_{fl} is the fluid density, $\rho = (1 - \phi)\rho_s + \phi\rho_{fl}$ is the bulk density, ρ_s is the mineral density,$\rho_1 = \rho_{fl}T/\phi + \eta/(i\omega\kappa)$, T is the tortuosity, ϕ the is porosity, and κ is the permeability. The P-wave velocity predicted by model 3 is consistent with Gassmann velocity at the low frequency limit. However, as model 2, the characteristic frequency of the squirt-flow dissipation peak has no dependence on the permeability.

2.4. Model 4

To obtain the new squirt-flow model, we apply the boundary condition of model 2 to model 1 (the boundary pressure at the junction of microfracyures and stiff pores is zero). In the in-situ subground porous rocks, especially for those deep reservoir rocks, the initial pore fluid pressure is in equilibrium between the soft and stiff pores, and it is not zero, but a constant pore pressure. The modified solid bulk modulus with a constant pore pressure is then (see Appendix A):

$$K_{ms} = K_{msd} + \frac{\alpha_c^2 F_c}{\phi_c}\left[1 - \frac{2J_1(\lambda R)}{\lambda R J_0(\lambda R)}\right], \tag{8}$$

where $F_c = (1/K_{fl} + 1/(\phi_c Q_c))^{-1}$. R is the characteristic squirt flow length. It indicates the relaxed distance of the fluid when the squirt flow occurs inside the rock. The modified dry-rock modulus is (see Appendix B)

$$\frac{1}{K_{md}} = \frac{1}{K_{ms}} + \frac{1}{K_{hp}} - \frac{1}{K_0}. \tag{9}$$

Mavko and Jizba (1991) showed that the shear modulus of the modified frame is

$$\frac{1}{\mu_{md}} = \frac{1}{\mu_{dry}} - \frac{4}{15}\left(\frac{1}{K_{dry}} - \frac{1}{K_{md}}\right). \tag{10}$$

According to Toksöz and Johnston (1981), the P-wave phase velocity and attenuation factor are

$$V_{phP1,2} = \frac{1}{\mathrm{Re}(X_{1,2})},\ a_{1,2} = \omega\,\mathrm{Im}(X_{1,2}), \tag{11}$$

where, $X_{1,2} = \sqrt{Y_{1,2}}$, $Y_{1,2} = -\frac{B}{2A} \pm \sqrt{\left(\frac{B}{2A}\right)^2 - \frac{C}{A}}$, $A = \frac{\phi F M_{dry}}{\rho_2^2}$, $B = \frac{F\left(2\alpha - \phi - \phi\frac{\rho_1}{\rho_2}\right) - \left(M_{dry} + F\frac{\alpha^2}{\phi}\right)\left(1 + \frac{\rho_a}{\rho_2} + i\frac{\omega_c}{\omega}\right)}{\rho_2}$, $C = \frac{\rho_1}{\rho_2} + \left(1 + \frac{\rho_1}{\rho_2}\right)\left(\frac{\rho_a}{\rho_2} + i\frac{\omega_c}{\omega}\right)$, $\rho_1 = (1 - \phi)\rho_s$, $\rho_2 = \phi\rho_{fl}$, where ρ_a is the additional coupling density, $\omega_c = \eta\phi/(\kappa\rho_{fl})$ is the characteristic frequency, M_{dry} is the uniaxial modulus of the rock skeleton at drained conditions, $\alpha = 1 - K_{md}/K_0$ is the poroelasticity coefficient and $F = (1/K_{fl} + (\alpha - \phi)/(\phi K_0))^{-1}$.

3. Examples

The rock properties are those of Carcione and Gurevich (2011): The porosity is 0.2, the dry-rock bulk modulus is 18 GPa, the Poisson ratio of rock frame is 0.15, the mineral density is 2650 kg/m^3, the bulk modulus of the mineral is 50 GPa, the permeability is 2 mD, the fluid density is 1040 kg/m^3, the fluid viscosity is 1 cP, the fluid bulk modulus is 2.25 GPa, the additional coupling density is 420 kg/m^3, the characteristic squirt-flow length is 4 mm, the fracture porosity is 0.0002, the high-pressure dry-rock bulk modulus is 20 GPa, and the crack aspect ratio is 0.0008.

3.1. Effect of permeability

Fig. 3a shows that the P-wave velocity predicted by model 1 is higher than the high limit value (the rock without compliant pores) at high frequencies, which is related to the inappropriate boundary condition used in this model. The results of model 4 show that as the frequency increases, the P-wave velocity approaches the high limit value as it should be. Fig. 3b shows the dissipation peaks, with the high-frequency one corresponding to the Biot classical loss mechanism.

The results of varying permeability, keeping constant the other properties, are shown in Fig. 4. Models 2 and 3 are affected by the Biot mechanism but no significant variation occurs in the location of the squirt-flow peak, since permeability is not explicitly incorporated into these models. Regarding model 4, the squirt-flow characteristic frequency moves to high frequencies with increasing permeability, in agreement with Dvorkin and Nur (1993) and Parra (1997). Moreover, model 4 is consistent with Gassmann modulus at low frequencies and the high-frequency modulus (cracks closed) at high frequencies.

3.2. Effect of the characteristic squirt-flow length

We keep constant all the properties and vary the characteristic squirt-flow length: 2, 4 and 6 mm. This is not explicitly incorporated in models 2 and 3. Fig. 5 compares the results of models 1 and 4. The squirt-flow peak moves towards the low frequencies with increasing squirt-flow length, consistent with BISQ model.

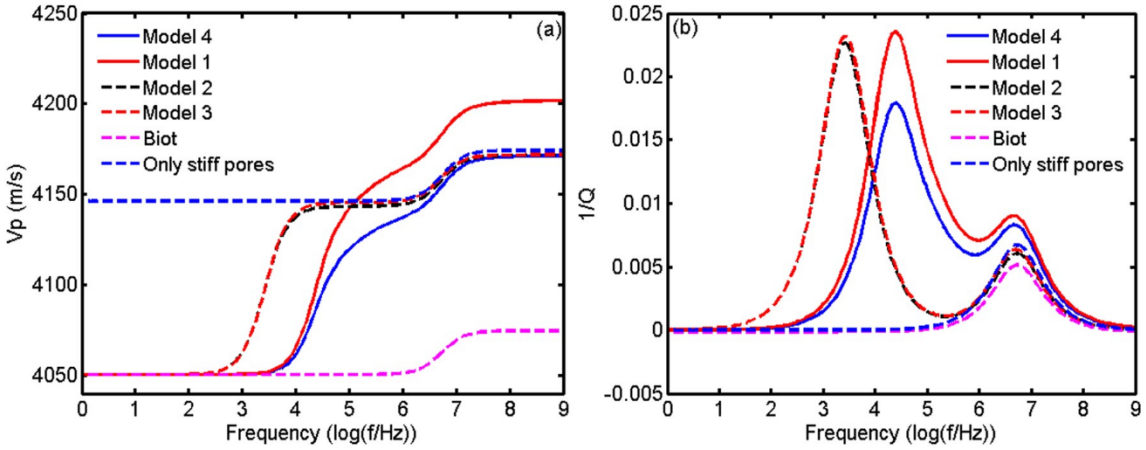

Fig. 3. P-wave velocity (a) and dissipation factor (b) as a function of frequency.

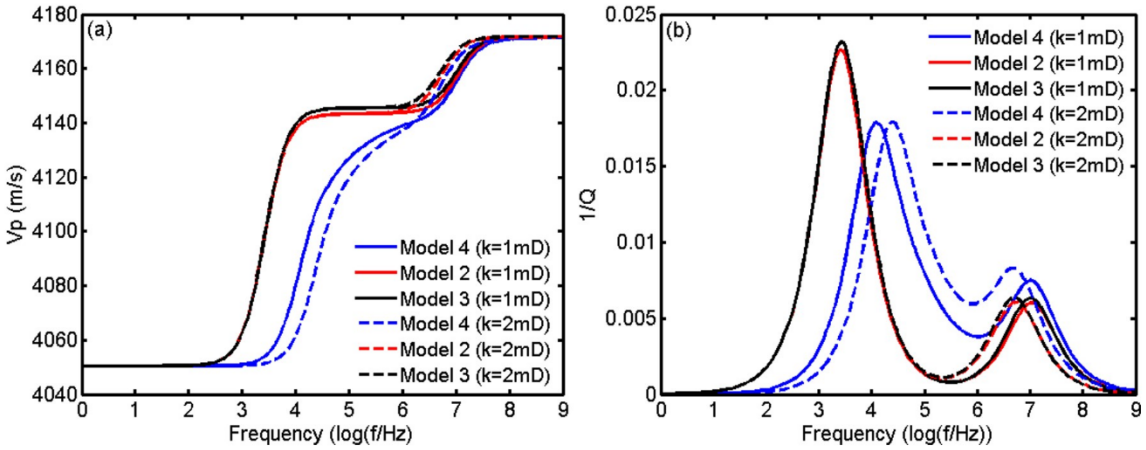

Fig. 4. Effect of permeability on (a) P-wave velocity, and (b) P-wave dissipation factor, as a function of frequency.

3.3. Effect of the fluid viscosity

As above, we keep all the properties constant but now vary the fluid viscosity: 1, 5 and 10 cP. The results are shown in Fig. 6. The squirt-flow characteristic frequency moves to the low frequencies as viscosity increases and the classical Biot peak to the opposite direction, as expected. Model 1 predicts a higher P-wave velocity at high frequencies compared to the other three models, and model 4 gives the weakest squirt-flow attenuation peak. The characteristic frequency predicted by models 2 and 3 is lower than that of model 1. The squirt-flow mechanism affects wave propagation at sonic-ultrasonic frequencies with a low fluid viscosity (Pride and Berryman, 2003; Pride et al., 2004; Deng et al., 2012).

4. Application to experimental data

We consider eight rocks of tight-sandstones, collected from a tight-gas reservoir of the Xujiahe formation in the Guang'an district of

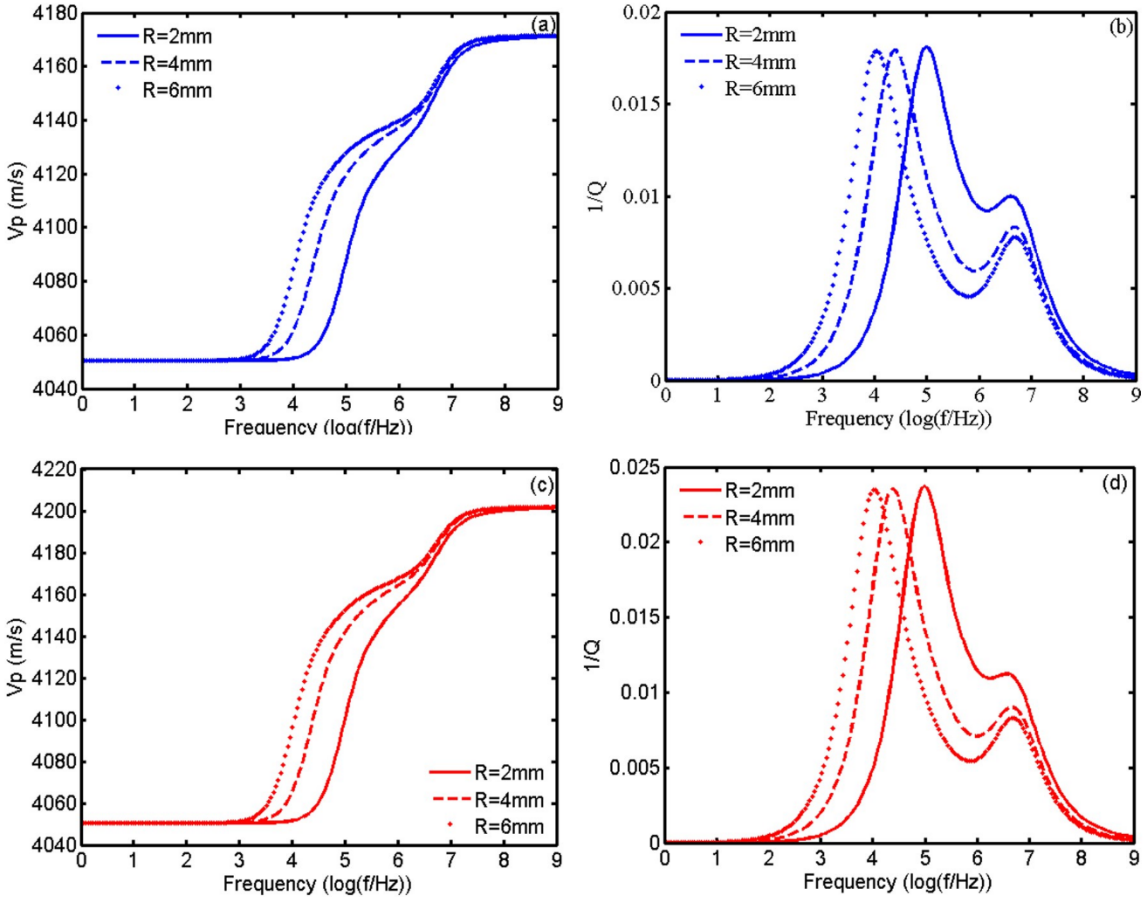

Fig. 5. Effect of the characteristic squirt-flow length on the fast P-wave velocity (a) and dissipation factor (b) as a function of frequency for model 4. Panels (c) and (d) correspond to model 1.

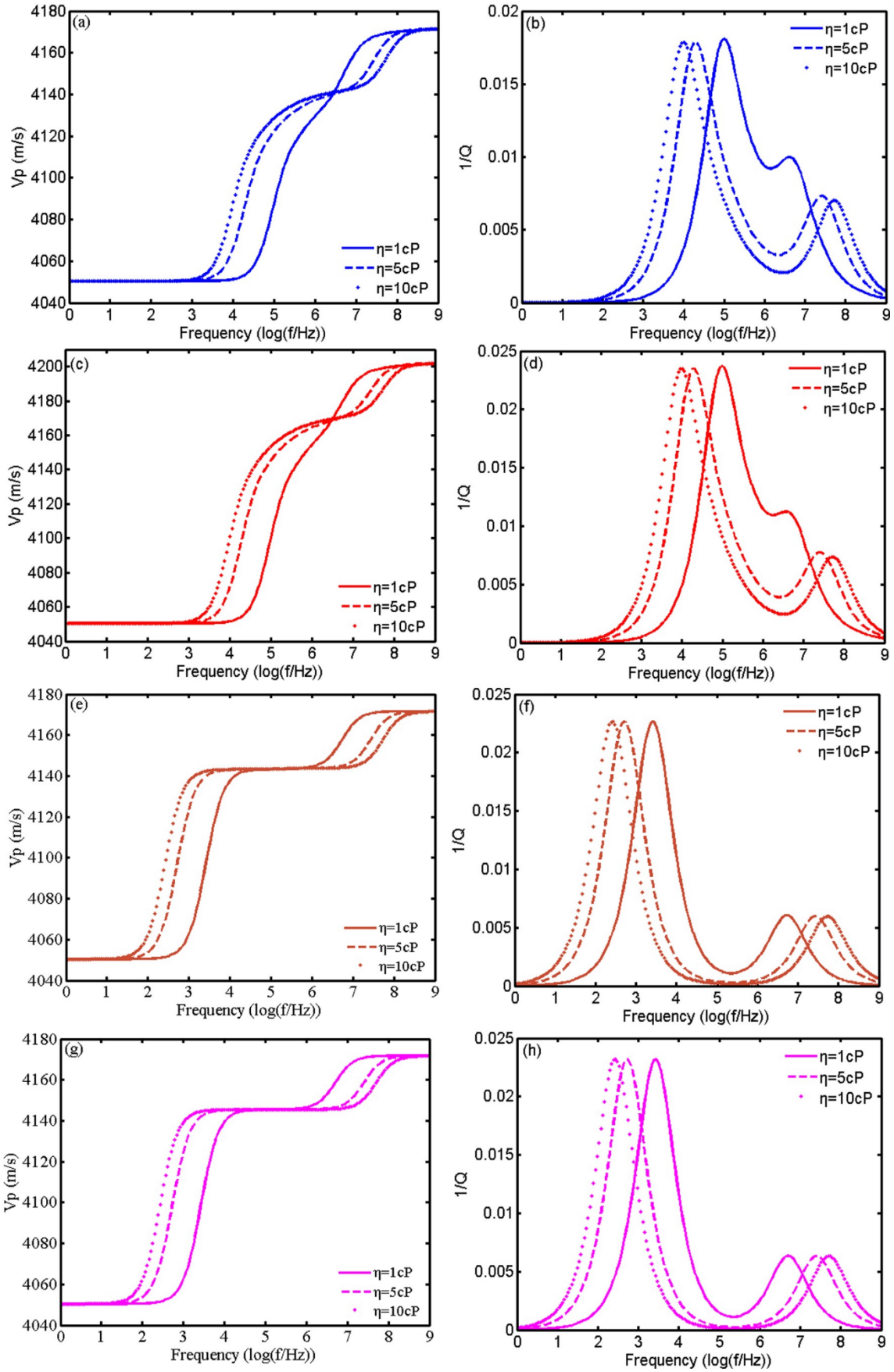

Fig. 6. Effect of the fluid viscosity on the fast P-wave velocity (a) and dissipation factor (b) as a function of frequency for model 4. Panels (c) and (d), (e) and (f) and (g) and (h) correspond to model 1, 2 and 3, respectively.

Table 1
Properties of the tight sandstones from the Guang'an district, Sichuan Basin.

Sample	Porosity (%)	Permeability (mD)	Grain density(kg/m^3)
GAR 11	3.03	0.001	2687
GA3	3.46	0.005	2694
GAR7	8.65	0.028	2668
GA6	6.26	0.046	2672
GAR6	6.33	0.047	2665
GA8	8.55	0.082	2670
GAR12	8.97	0.14	2662
GA1	13.26	1.21	2659

Sichuan Basin, southwest China. Rock porosity ranges from 3 to 14%, and the permeability from 0.001 to 1.21 mD. The experimental set-up is that described by Guo et al. (2009). Differential pressures from 5 to 35 MPa are applied to each sample at 80 °C. The measurements were performed at full gas and water saturations. The rock properties are given in Table 1 (the mineral bulk modulus is assumed to be 39 GPa). The wave velocities are represented in Fig. 7. Both the P- and S-wave velocities increase with confining pressure and, for the same sample and pressure, the P-wave velocity at full water saturation is higher than that at full gas saturation.

The characteristic squirt-flow length is assumed to be of the order of the average pore size (Dvorkin and Nur, 1993). Diallo and Appel (2000) and Diallo et al. (2003) proposed a model which does not require the characteristic squirt-flow length, but their predicted P-wave velocity dispersion and attenuation move to the high frequencies as the permeability decreases, which is not consistent with the other models (Dvorkin and Nur, 1993; Parra, 1997).

Fig. 8 compares the results with the experimental data for different flow lengths. The dry-rock bulk and shear moduli are determined by the Gassmann theory based on the measured P- and S-wave velocities at full gas saturation. The rock properties are those of Table 1 and the fluid properties are obtained at the measurement conditions according to Batzle and Wang (1992). The predicted P-wave velocity increases with the characteristic squirt-flow length at each differential pressure. The comparison reveals that the appropriate flow length decreases as the pressure increases (see Fig. 8 (a, c, e–h)) except for the GA3 and GA6 samples (see Fig. 8 (b, d)). Part of the microfractures with lower aspect ratio tend to close as the confining pressure increases, resulting in a reduction of the characteristic squirt-flow length in some samples.

The model 4 is used to predict the P-wave velocity with a constant characteristic squirt flow length (by considering it as an intrinsic rock property) under the differential confining pressures. Based on the theoretical predictions, the characteristic squirt flow length can be determined by fitting the experimental data. Fig. 9 shows the characteristic squirt-flow length as a function of permeability and porosity for the eight rock samples. It is in the range 0.015 to 0.350 mm, and apparently, it increases with increasing permeability or porosity. Dvorkin and Nur (1993) suggested that the flow length can be considered an intrinsic property of rocks. Based on a statistical analysis on sets of experimental measurements, Cheng et al. (2019) showed that the crack fraction and its radius increases with total porosity in low to moderate porosity sandstones. Consequently, a higher crack fraction and flow length enhance the effect of local fluid flow induced by the waves.

5. Conclusions

We combined two different squirt-flow theories to correctly model the low- and high-frequency limits of the P-wave velocity and the effects of permeability on wave propagation, namely velocity dispersion and dissipation. The examples show that the predicted P-wave attenuation peak moves to the low frequencies with increasing characteristic squirt-flow length or fluid viscosity, and to the high frequencies with increasing permeability. An application of the model to experimental data (tight sandstones) shows that the characteristic squirt-flow length decreases with increasing confining pressure and increases with increasing porosity or permeability. The squirt-flow effect is stronger with increasing porosity, due to the increase in crack fraction with porosity in low and moderate porosity sandstones.

CRediT authorship contribution statement

Chunfang Wu:Conceptualization, Data curation, Formal analysis, Methodology, Writing - original draft.**Jing Ba**:Conceptualization, Formal analysis, Funding acquisition, Methodology, Project administration, Supervision, Writing - original draft, Writing - review & editing.**José M. Carcione**:Methodology, Supervision, Validation, Writing - review & editing.**Li-Yun Fu**:Investigation, Project administration, Resources, Writing - review & editing.**Evgeni M. Chesnokov**:Resources, Supervision, Validation.**Lin Zhang**:Data curation, Validation, Writing - review & editing.

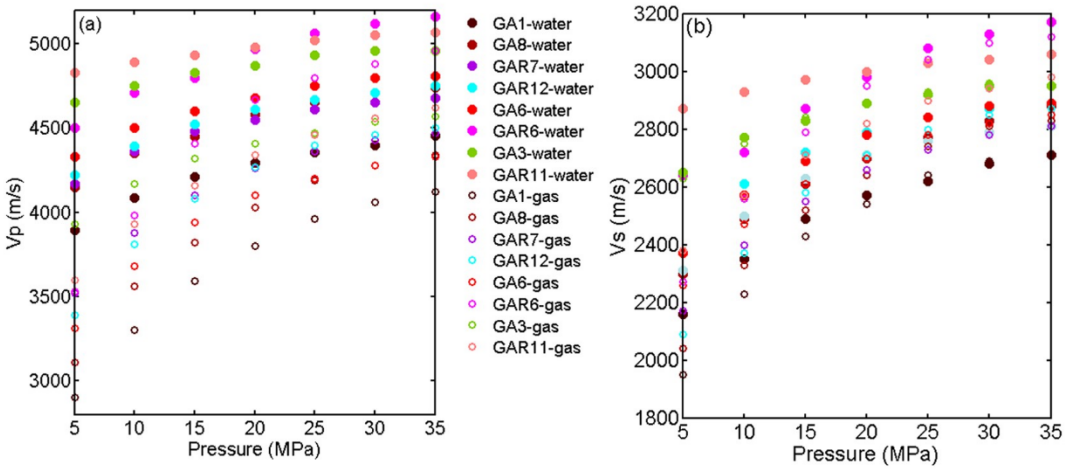

Fig. 7. Experimental P- and S-wave phase velocities (a and b) as a function of the differential pressure.

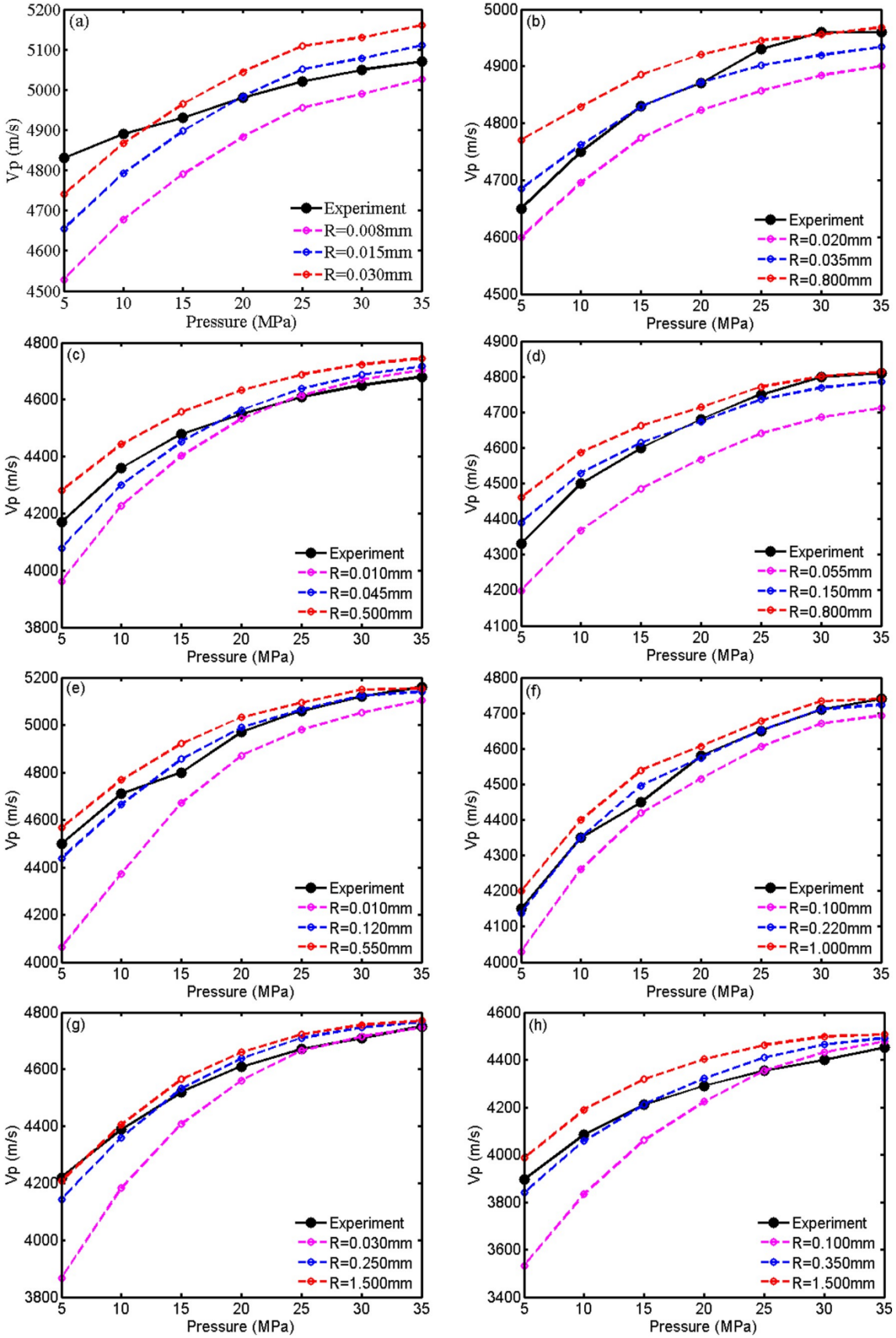

Fig. 8. Predicted P-wave velocities compared with the experimental data for different characteristic squirt-flow lengths; (a) GAR11, (b) GA3, (c) GAR7, (d) GA6, (e) GAR6, (f) GA8, (g) GAR12, (h) GA1.

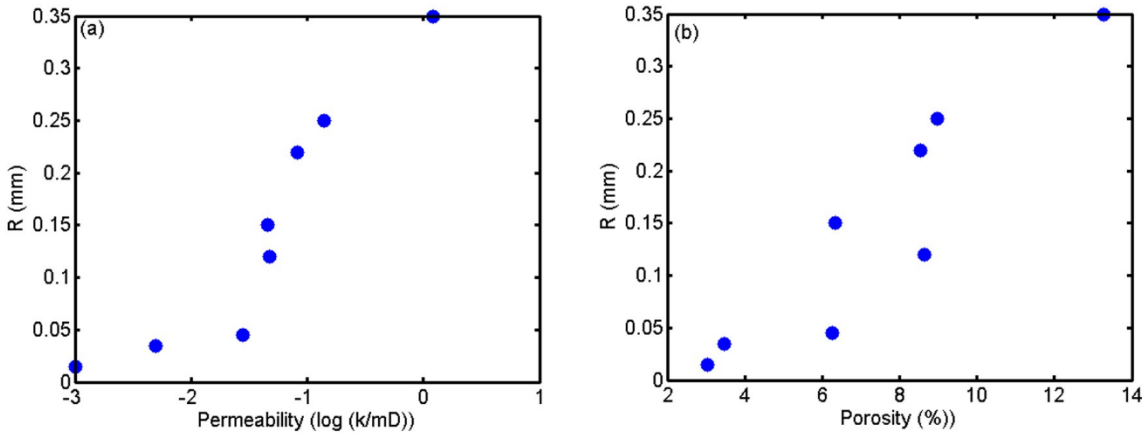

Fig. 9. Characteristic squirt-flow length as a function of permeability (a) and porosity (b).

Declaration of competing interest

The authors declare that to their knowledge they have no personal interest or relations with academic or private Institutions that may have influenced the contents of this paper.

Acknowledgements

This work is supported by the China Scholarship Council (File no. 201806710037), Jiangsu Innovation and Entrepreneurship Plan, Specially-Appointed Professor Program of Jiangsu Province and the National Natural Science Foundation of China (grant no. 41974123).

Appendix A. Modified solid bulk modulus

According to Dvorkin and Nur (1993), we assume an ideal cylinder with radius R. Biot (1941) and Rice and Cleary (1976) provide the relationship among the skeleton deformation ($e = du/dx$), fracture porosity and pore pressure as

$$\frac{\partial \phi_c}{\partial t} = \alpha_c \frac{\partial e}{\partial t} + \frac{1}{Q_c}\frac{\partial P}{\partial t}, \tag{A1}$$

$$\mathrm{d}\rho_{fl} = \frac{\mathrm{d}p}{c_0^2}, \tag{A2}$$

where u is the solid displacement, c_0 is the fluid sound velocity, $\alpha_c = 1 - K_{msd}/K_0$, and $Q_c = K_0/(\alpha - \phi_c)$. The relation given by Dvorkin et al. (1995) is $K_{msd} = (1/K_0 - 1/K_{hp} + 1/K_{dry})^{-1}$.

We assume that the fluid inside the crack can only flow in the radial direction r. Therefore, the fluid mass conservation equation is

$$\frac{1}{\rho_{fl}}\frac{\partial \rho_{fl}}{\partial t} + \frac{1}{\phi_c}\frac{\partial \phi_c}{\partial t} + \frac{\partial}{\partial t}\left(\frac{\partial w}{\partial r} + \frac{w}{r}\right) = 0 \tag{A3}$$

where t is time and w is fluid displacement.

Substituting Eqs. (A1) and (A2) into (A3), we obtain

$$\frac{1}{\rho_{fl}c_0^2}\frac{\partial p}{\partial t} + \frac{1}{\phi_c}\left(\alpha_c\frac{\partial e}{\partial t} + \frac{1}{Q_c}\frac{\partial p}{\partial t}\right) + \frac{\partial}{\partial t}\left(\frac{\partial w}{\partial r} + \frac{w}{r}\right) = 0 \tag{A4}$$

The relation between fluid oscillation speed and pore pressure gradient can be derived by the Darcy's law.

$$\frac{\partial w}{\partial t} = -\frac{\kappa}{\eta\phi_c}\frac{\partial p}{\partial r}. \tag{A5}$$

We assume that the parameters are time-harmonic as

$$\exp(-i\omega t). \tag{A6}$$

Substituting Eq. (A6) into (A4) and (A5) gives

$$\left(\frac{1}{K_{fl}} + \frac{1}{\phi_c Q_c}\right)P + \frac{\alpha_c e}{\phi_c} + \frac{\partial w}{\partial r} + \frac{w}{r} = 0, \tag{A7}$$

$$w = \frac{\kappa}{i\omega\eta\phi_c}\frac{\partial p}{\partial r}. \tag{A8}$$

According to Eqs. (A7) and (A8), the differential equation for $_P$ is

$$\frac{d^2p}{dr^2} + \frac{1}{r}\frac{dp}{dr} + \frac{i\omega\eta\phi_c}{\kappa}\left(\frac{1}{K_{fl}} + \frac{1}{\phi_c Q_c}\right)P = -e\frac{\alpha_c}{\phi_c}\frac{i\omega\eta\phi_c}{\kappa}. \tag{A9}$$

At the fracture boundary, the pressure is always constant ($dp = 0$).

The solution is

$$P = -e\frac{\alpha_c}{\phi_c}\frac{1}{\frac{1}{K_{fl}}+\frac{1}{\phi_c Q_c}}\left[1-\frac{J_0(\lambda r)}{J_0(\lambda R)}\right], \tag{A10}$$

where $\lambda^2 = i\omega\mu\phi_c/\kappa(1/K_{fl} + 1/(\phi_c Q_c))$.

The average fluid pressure is

$$P_{av} = \frac{1}{\pi R^2}\int_0^R 2\pi r P(r)dr = -e\frac{\alpha_c}{\phi}\frac{1}{\frac{1}{K_{fl}}+\frac{1}{\phi_c Q_c}}\left[1-\frac{2J_1(\lambda R)}{\lambda R J_0(\lambda R)}\right]. \tag{A11}$$

Biot (1941), Rice and Cleary (1976), and Dvorkin and Nur (1993) established the relation between the external stress, displacement and pore pressure in rocks. Therefore, in the modified solid, the external stress is related to the deformation and average pore pressure as

$$d\sigma = K_{msd}de - \alpha_c dp_{av}. \tag{A12}$$

The modified solid bulk modulus is

$$K_{ms} = \frac{d\sigma}{de}. \tag{A13}$$

Substituting Eqs. (A11) and (A12) into Eq. (A13) gives

$$K_{ms} = K_{msd} + \frac{\alpha_c{}^2 F_c}{\phi_c}\left[1-\frac{2J_1(\lambda R)}{\lambda R J_0(\lambda R)}\right]. \tag{A14}$$

Appendix B. Bulk modulus of the modified skeleton

The relation between the dry pore volume, the bulk modulus of the mineral mixture and the bulk modulus of the rock frame is (Walsh, 1965)

$$\frac{1}{K_{dry}} - \frac{1}{K_0} = \frac{1}{V}\frac{dVp}{d\sigma}, \tag{B1}$$

where V is the total volume of the rock, and $Vp$is the dry pore volume. This relation is applied to the modified rock frame,

$$\frac{1}{K_{md}} - \frac{1}{K_{ms}} = \frac{1}{V}\frac{dVp_{stiff}}{d\sigma}, \tag{B2}$$

where Vp_{stiff} is the volume of the stiff pores.

According to Mavko and Jizba (1991), the cracks close at a very high pressure, so that the bulk modulus of the modified solid can be obtained as

$$\frac{1}{K_{hp}} - \frac{1}{K_0} = \frac{1}{V}\frac{dVp_{stiff}}{d\sigma}, \tag{B3}$$

with Eqs. (B2) and (B3), the bulk modulus of the modified rock (dry) is

$$\frac{1}{K_{md}} = \frac{1}{K_{ms}} + \frac{1}{K_{hp}} - \frac{1}{K_0}. \tag{B4}$$

References

Ba, J., Carcione, J.M., Nie, J., 2011. Biot-Rayleigh theory of wave propagation in double-porosity media: Journal of Geophysical Research 116, B06202. https://doi.org/10.1029/2010JB008185.

Ba, J., Zhang, L., Sun, W., Hao, Z., 2014. Velocity field of wave-induced local fluid flow in double-porosity media. Science China Physics Mechanics & Astronomy 57, 1020–1030. https://doi.org/10.1007/s11433-014-5442-0.

Ba, J., Xu, W., Fu, L., Carcione, J.M., Zhang, L., 2017. Rock anelasticity due to patchy-saturation and fabric heterogeneity: a double-double porosity model of wave propagation: Journal of Geophysical Research. Solid Earth 122 (3), 1949–1976. https://doi.org/10.1002/2016JB013882.

Ba, J., Ma, R., Carcione, J.M., Picotti, S., 2019. Ultrasonic wave attenuation dependence on saturation in tight oil siltstones. J. Pet. Sci. Eng. 179, 1114–1122. https://doi.org/10.1016/j.petrol.2019.04.099.

Batzle, M., and Z. Wang, 1992, Seismic properties of pore fluids: Geophysics, **57**, no. 11, 1396–1408. doi:https://doi.org/10.1190/1.1443207.

Berryman, J.G., 2007. Seismic waves in rocks with fluids and fractures. Geophysical Journal International 171 (2), 954–974. https://doi.org/10.1111/j.1365-246X.2007.03563.x.

Biot, M.A., 1941. General theory of three-dimensional consolidation. J. Appl. Phys. 12, 155–164. https://doi.org/10.1063/1.1712886.

Biot, M.A., 1956a. Theory of propagation of elastic waves in a fluid-saturated porous solid. I: Low frequency range: The Journal of the Acoustical Society American 28, 168–178. https://doi.org/10.1121/1.1908239.

Biot, M.A., 1956b. Theory of propagation of elastic waves in a fluid-saturated porous solid. II: Higher frequency range: The Journal of the Acoustical Society American 28, 179–191. https://doi.org/10.1121/1.1908241.

Biot, M. A., 1962, Mechanics of deformation and acoustic propagation in porous media: Journal of Applied Physics, **33**, no. 4, 1482-1498, doi:https://doi.org/10.1063/1.1728759.

Carcione, J. M., 2014, Wave fields in real media. Theory and numerical simulation of wave propagation in anisotropic, anelastic, porous and electromagnetic media (third edition): Elsevier.

Carcione, J. M., and B. Gurevich, 2011, Differential form and numerical implementation of Biot's poroelasticity equations with squirt dissipation: Geophysics, **76**, no. 6, N55-N64 doi:https://doi.org/10.1190/geo2010-0169.1.

Cheng, W., J. Ba, L. Fu, and M. Lebedev, 2019, Wave-velocity dispersion and rock microstructure: Journal of Petroleum Science and Engineering, 183, 106466, doi:https://doi.org/10.1016/j.petrol.2019.106466.

Coyner, K. B., 1984, Effects of stress, pore pressure, and pore fluids on bulk strain, velocity, and permeability in rocks: Ph.D. thesis, Massachusetts Institute of Technology.

Deng, J. X. S. Wang, and W. Du, 2012, A study of the influence of mesoscopic pore fluid flow on the propagation properties of compressional wave-a case of periodic layered porous media: Chinese Journal of Geophysics (in Chinese), **55**, no. 8, 2716–2727, doi:https://doi.org/10.6038/j.issn.0001-5733.2012.08.024.

Diallo, M. S., and E. Appel, 2000, Acoustic wave propagation in saturated porous media: reformulation of the Biot/Squirt-flow theory: Journal of Appiled Geophysics, **44**, no. 4, 313–325, doi:https://doi.org/10.1016/S0926-9851(00)00009-4.

Diallo, M. S., M. Prasad, and E. Appel, 2003, P-wave velocity and attenuation at ultrasonic frequency: Wave Motion, **37**, no. 1, 1-16, doi:https://doi.org/10.1016/S0165-2125(02)00018-5.

Dvorkin, J., and A. Nur, 1993, Dynamic poroelasticity: a unified model with the squirt

and the Biot mechanics: Geophysics, **58**, no. 4, 524–533, doi:https://doi.org/10.1190/1.1443435.

Dvorkin, J., R. Nolen-Hoeksema, and A. Nur, 1994, The squirt-flow mechanism: macroscopic description: Geophysics, **59**, no. 3, 428–438, doi:https://doi.org/10.1190/1.1443605.

Dvorkin, J., G. Mavko, and A. Nur, 1995, Squirt flow in fully saturated rocks: Geophysics, **60**, no. 1, 97–107, doi:https://doi.org/10.1190/1.1443767.

Gassmann, F., 1951. Über die Elasticität Poröser Medien: Vierteljahrsschrift: der Naturforschenden Gesellschaft Zürich 96, 1–23.

Guo, M., L. Fu, and J. Ba, 2009, Comparison of stress-associated coda attenuation and intrinsic attenuation from ultrasonic measurements: Geophysical Journal International, **178**, no. 1, 447–456, doi:https://doi.org/10.1111/j.1365-246X.2009.04159.x.

Gurevich, B., D. Makarynska, and M. Pervukhina, 2009, Ultrasonic moduli for fluid-saturated rocks: Mavko-Jizba relations rederived and generalized: Geophysics, **74**, no. 4, N25-N30, doi:https://doi.org/10.1190/1.3123802.

Gurevich, B., D. Makarynska, O. B. de Paula, and M. Pervukhina, 2010, A simple model for squirt-flow dispersion and attenuation in fluid-saturated granular rocks: Geophysics, **75**, no. 6, N109-N120, doi:https://doi.org/10.1190/1.3509782.

Han, D., 1986, Effects of porosity and clay content on acoustic properties of sandstones and unconsolidated sediments: Ph.D. dissertation, Stanford University.

Han, D., A. Nur, and D. Morgan, 1986, Effects of porosity and clay content on wave velocities in sandstones: Geophysics, **51**, no. 11, 2093–2107, doi:https://doi.org/10.1190/1.1893163.

Markova, I., G. R. Jarillo, M. Markov, and B. Gurevich, 2014, Squirt flow influence on sonic log parameters: Geophysical Journal International, **196**, no. 2, 1082–1091, doi:https://doi.org/10.1093/gji/ggt442.

Mavko, G., and D. Jizba, 1991, Estimating grain-scale fluid effects on velocity dispersion in rocks: Geophysics, **56**, no. 12, 1940–1949, doi:https://doi.org/10.1190/1.1443005.

Mavko, G., and D. Jizba, 1994, The relation between seismic P-and S-wave velocity dispersion in saturated rocks: Geophysics, **59**, no. 1, 87–92, doi:1190/1.1443537.

Müller, T. M., B. Gurevich, and M. Lebedev, 2010, Seismic wave attenuation and dispersion due to wave-induced flow in porous rocks - A review: Geophysics, **75**, no. 5, A147-A164, doi:https://doi.org/10.1190/1.3463417.

Murphy, W. F., K. W. Winkler, and R. L. Kleinberg, 1986, Acoustic relaxation in sedimentary rocks, dependence on grain contacts and fluid saturation: Geophysics, **51**, no. 3, 757–766, doi:https://doi.org/10.1190/1.1442128.

Parra, J.O., 1997. The transversely isotropic poroelastic wave equation including the Biot and the squirt mechanisms: theory and application. Geophysics 62 (1), 309–319. https://doi.org/10.1190/1.1444132.

Pride, S.R., Berryman, J.G., 2003. Linear dynamic of double-porosity dual-permeability materials. I. Govering equations and acoustic attenuation: Physical Review E 68, 036603.

Pride, S.R., Berryman, J.G., Harris, J.M., 2004. Seismic attenuation due to wave-induced flow: Journal of Geophysical 109, B01201. https://doi.org/10.1029/2003JB002639.

Rice, J.R., Cleary, M.P., 1976. Some basic stress diffusion solutions for fluid-saturated elastic porous media with compressible constituents. Rev. Geophys. 14, 227–241. https://doi.org/10.1029/RG014i002p00227.

Tang, X., X. Chen, and X. Xu, 2012, A cracked porous medium elastic wave theory and its application to interpreting acoustic data from tight formations: Geophysics, **77**, no. 6, D245-D252, doi:https://doi.org/10.1190/geo2012-0091.1.

Toksöz, M. N., and D. H. Johnston, 1981, Seismic wave attenuation: Geophysics reprint series, no. 2, Society of Exploration Geophysicists.

Walsh, J.B., 1965. The effect of cracks on the compressibility of rock. J. Geophys. Res. 70, 381–389. https://doi.org/10.1029/JZ070i002p00381.

Wang, Z., and A. Nur, 1990, Dispersion analysis of acoustic velocities in rocks: Journal of Acoustical Society of America, **87**, no. 6, 2384-2395, doi:https://doi.org/10.1121/1.399551.

Winkler, K.W., 1983. Frequency dependent ultrasonic properties of high-porosity sandstones. J. Geophys. Res. 88, 9493–9499. https://doi.org/10.1029/JB088iB11p09493.

Yang, D., and Z. Zhang, 2000, Effects of the Biot and the Squirt-flow coupling interaction on anisotropic elastic waves: Chinese Science Bulletin, **45**, no. 23, 2130-2138, doi:https://doi.org/10.1007/BF02886316.

Yang, D., and Z. Zhang, 2002, Poroelastic wave equation including the Biot/Squirt mechanism and the solid/fluid coupling anisotropy: Wave motion, **35**, no. 3, 223-245, doi:https://doi.org/10.1016/S0165-2125(01)00106-8.

Yao, Q., D. Han, F. Yan, and L. Zhao, 2015, Modeling attenuation and dispersion in porous heterogeneous rocks with dynamic fluid modulus: Geophysics, **80**, no. 3, D183-D194, doi:https://doi.org/10.1190/geo2013-0410.1.

Zhang, L., Ba, J., Fu, L., Carcione, J.M., Cao, C., 2019. Estimation of pore microstructure by using the static and dynamic moduli. Int. J. Rock Mech. Min. Sci. 113, 24–30. https://doi.org/10.1016/j.ijrmms.2018.11.005.